

From micro to reservoir scale: Permeability from digital experiments

JACK DVORKIN, *Stanford University*

NAUM DERZHI, QIAN FANG, AMOS NUR, BOAZ NUR, AVRAMI GRADER, CHUCK BALDWIN, HENRIQUE TONO, and ELIZABETH DIAZ, *Ingrain*

Absolute and relative permeability are key inputs into reservoir flow simulation. The other two key inputs are porosity and hydrocarbon saturation. Porosity can be, in principle, inferred from acoustic impedance if an impedance-porosity transform is available. Such transforms can be obtained from sonic, density, and porosity data at a well. Typically, a theoretical rock physics model is found to explain these data and then used to expand the impedance-porosity interpretation beyond the data range present in the well. Saturation volumes emerge from reservoir modeling itself if the initial distribution of fluids is specified. However, the permeability required to arrive at fluid distribution in the reservoir versus time and for given boundary conditions remains, by and large, unknown.

Definitions, equations, and examples: Permeability and elastic properties

The absolute permeability $k_{Absolute}$ is defined from Darcy's equation

$$Q = -k_{Absolute} \frac{A}{\mu} \frac{dP}{dx}, \quad (1)$$

where Q is the volume flux through the sample (m^3/s); A is the cross-sectional area of the sample (m^2); μ is the dynamic viscosity of the fluid ($Pa \cdot s$ with $1 \text{ cPs} = 10^{-3} \text{ Pa} \cdot s$); and dP/dx is the pressure drop across the sample divided by the length of the sample (Pa/m).

Theoretically, the absolute permeability depends only on the pore-space geometry but not on the pore fluid (notice that the right side of Equation 1 is normalized by the viscosity). Practically, in the physical laboratory, it is measured by applying a pressure head (dP) to a cylindrically-shaped sample along its central axis and measuring the resulting flux (Q). The $k_{Absolute}$ thus obtained may depend on the fluid type (e.g., water versus oil versus air). This may happen for several reasons including the following: (a) the grains may be water-wet rather than oil- or gas-wet and, as a result, residual water remains in the pores in the presence of hydrocarbons; or (b) the introduction of a fluid alters the sample by, e.g., forcing clays to swell; or (c) the compressible nature of gas flow where the volumetric output is different from the input at a strong pressure head.

A simple and powerful equation to estimate $k_{Absolute}$ is the Mavko-Nur (1997) modification of the Kozeny-Carman equation:

$$k_{Absolute} = \frac{d_{Mean}^2}{72\tau^2} \frac{(\phi - \phi_p)^3}{[1 - (\phi - \phi_p)]^2} \quad (2)$$

where d_{Mean} is the mean grain size; τ is the tortuosity; ϕ is the total porosity; and ϕ_p is the percolation porosity (porosity at

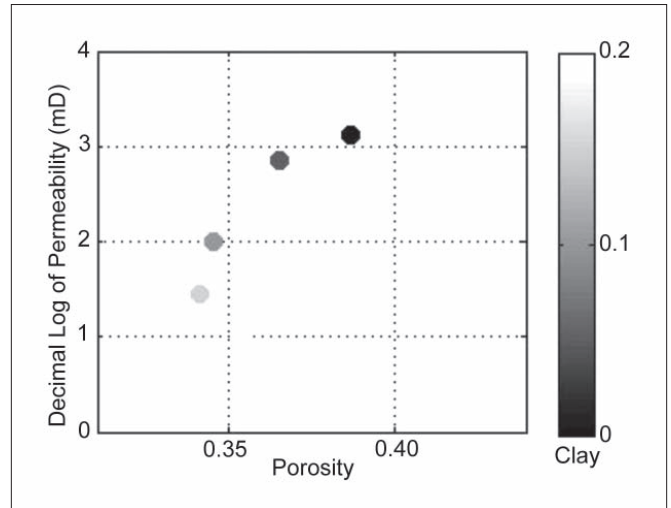


Figure 1. Decimal logarithm of absolute permeability in a mixture of Ottawa sand and kaolinite color-coded by the kaolinite content. Value 3 on the vertical axis is for 1000 mD while 1 is for 10 mD.

which the pore space becomes disconnected and, hence, permeability becomes zero). The permeability from Equation 2 has the same units as d_{Mean}^2 . This means that if d_{Mean} is in m, $k_{Absolute}$ is in m^2 . To translate these units into more conventional units of millidarcy (mD), use $1 \text{ mD} = 10^{-15} \text{ m}^2$.

Timur introduced one of the most commonly used equations that link the absolute permeability to porosity ϕ and irreducible water saturation S_{wi} :

$$k_{Absolute} = 8581\phi^{4.4} / S_{wi}^2 \quad (3)$$

where ϕ and S_{wi} are in unitless volume fractions and $k_{Absolute}$ is in mD.

This is a purely empirical equation in which the units of the variables are not internally consistent. Nevertheless, we can use it to calculate the irreducible water saturation from the permeability (in mD) given by Equation 2 as

$$S_{wi} = 93\phi^{2.2} / \sqrt{k_{Absolute}} \quad (4)$$

where the units are the same as in Equation 3.

Where the sediment contains particles of drastically different sizes (like sand and shale), we assume that the mean grain size d_{Mean} used in Equation 2 is the harmonic average of those of the sand d_{Sand} and shale d_{Shale} (Mavko et al., 2009):

$$d_{Mean}^{-1} = (1 - C)d_{Sand}^{-1} + Cd_{Shale}^{-1} \quad (5)$$

where C is the shale content. To ascertain how $k_{Absolute}$ can change versus C , consider data from Ottawa sand and kaolin-

ite mixtures (Yin, 1992) shown in Figure 1.

Relative permeability is used to quantify multiphase flow, such as the flow of oil in the presence of water and water in the presence of oil. In a sample with two such fluids, the relative permeabilities k_{ro} and k_{rw} , by definition, are

$$k_{ro} = - \frac{Q_o \mu_o}{k_{Absolute} AdP/dx}, \quad k_{rw} = - \frac{Q_w \mu_w}{k_{Absolute} AdP/dx}, \quad (6)$$

where the subscripts “o” and “w” refer to oil and water, respectively. The fluxes Q_o and Q_w are measured at fixed water saturation S_w . Relative permeability is usually plotted versus S_w . Because these fluxes of the fluid phases at partial saturation are smaller than the flux measured in a sample fully saturated with water or oil, the relative permeability is always smaller than 1 and larger than or equal to 0. Typical k_{ro} and k_{rw} versus S_w curves produced by digital two-phase flow simulations are displayed in Figure 2. They are very similar to those obtained in the physical laboratory.

The relative permeability depends on more factors than $k_{Absolute}$, including the wettability of the minerals, interfacial surface tension, and viscosity contrast between the fluid phases. These parameters may vary in space and time, the latter due to pressure, flow, and the resulting hydrocarbon state and composition changes during production.

Consider next an elastic property model appropriate for unconsolidated soft sediment, the “soft sand” or modified lower Hashin-Strikman transform (Mavko et al., 2009). Figure 3 displays the impedance versus porosity and impedance versus Poisson’s ratio for a sand/clay mixture with the clay content between 5 and 15%. These calculations are conducted for sediment with full water saturation as well as for partial water saturations of 70% and 30%. The rest of the pore space is occupied by light oil.

If the pore fluids and their in-situ contents are known and the clay content is within a narrow range, the porosity can be inferred from the impedance with reasonable accuracy. Yet such an interpretation has well-known uncertainties: (a) sediment with oil and water can be differentiated from that with 100% water using the elastic impedance (Poisson’s ratio), but it is difficult to quantify the oil saturation; (b) the clay content is uncertain; and (c) the scale of rock physics models is finer than that of seismic images, which means that if a feature is below seismic resolution its seismically derived elastic properties are influenced by the surroundings.

The uncertainty issue can be dealt with either on a rigorous probabilistic basis (Avseth et al., 2005) or by simply using the “what if” approach where the inputs are given a few plausible variants and the resulting rock property scenarios

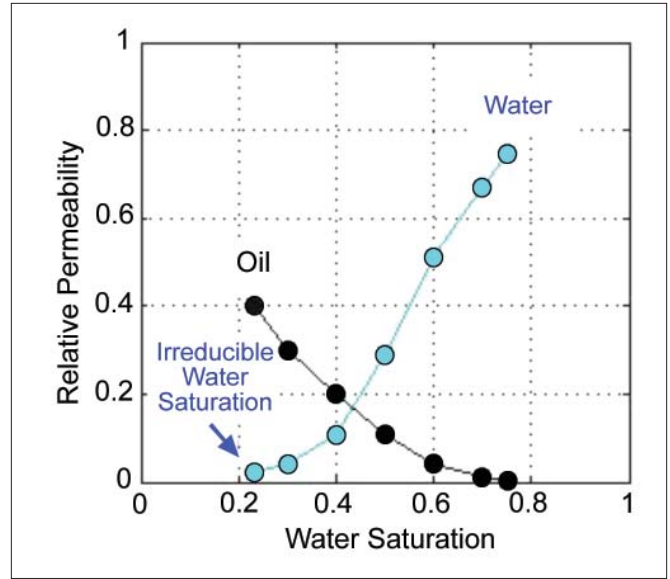


Figure 2. Relative permeability curves. The permeability to oil at the irreducible water saturation is about 40% of the absolute permeability. These curves come from digital simulations.

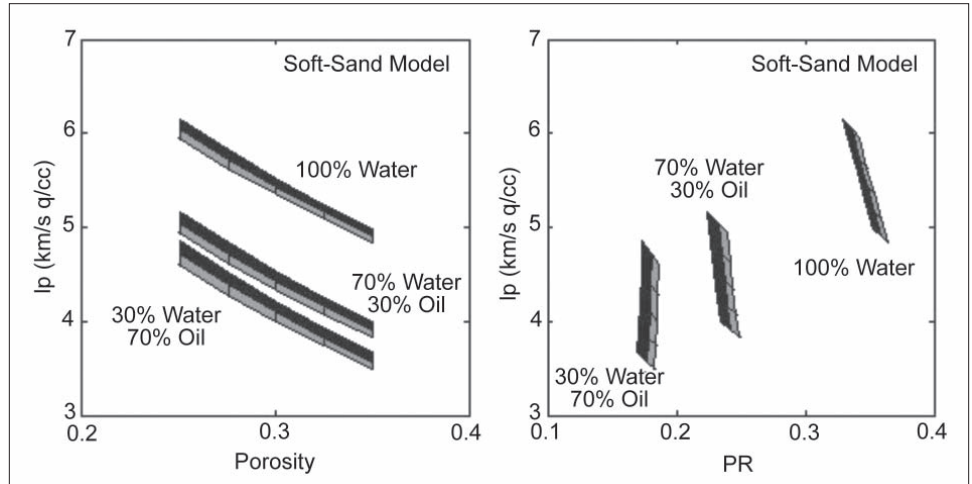


Figure 3. Soft-sand model. Impedance versus porosity (left) and versus Poisson’s ratio (right), color-coded by the clay content. Darker stripes are for 5% clay content while lighter stripes are for 15% clay content. The three bands are for full water saturation and 70% and 30% water saturations.

are determined. The scale issue is arguably not very important for large geobodies and can be addressed by operating with averaged (or upscaled) rock properties (e.g., Dvorkin and Nur, 2009).

What remains extremely uncertain is the permeability that necessarily has to be supplied in reservoir modeling. This is because even if Equation 2 is used to link permeability to porosity, the former is proportional to the grain size squared—a parameter that is quite difficult to determine.

Essentiality of permeability

To illustrate this latest point, consider a simple Earth model where a high-porosity turbiditic channel is embedded in shale (Figure 4). The porosity in the channel slightly diminishes in the direction of debris flow and the corresponding shale (or clay) content increases from 5 to 15%. The porosity

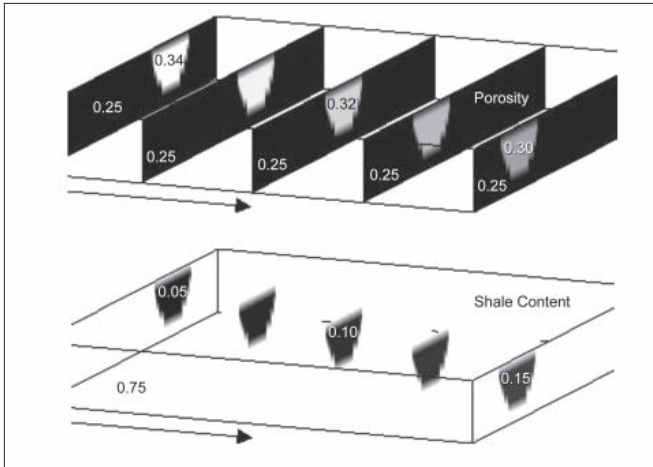


Figure 4. Porosity (top) and shale content (bottom) in an idealized channel and surrounding shale. The direction of depositional flow is marked by the arrows.

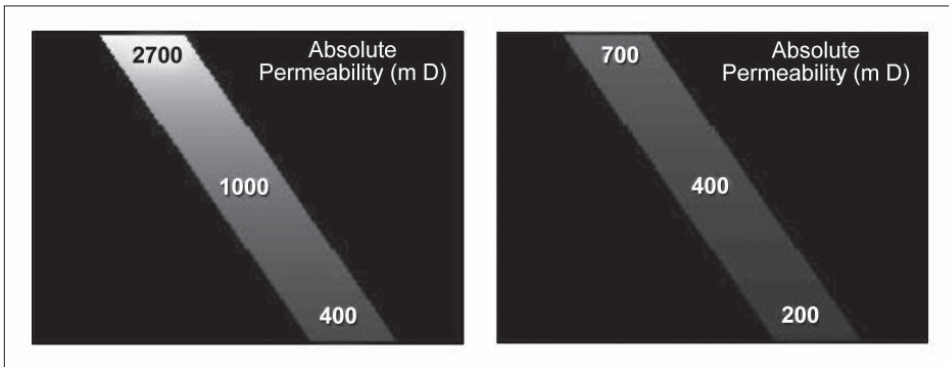


Figure 5. Absolute permeability at the top of the channel for two sand-grain size scenarios: 0.4 mm (left) and 0.1 mm (right). The direction of depositional flow is from top left to bottom right.

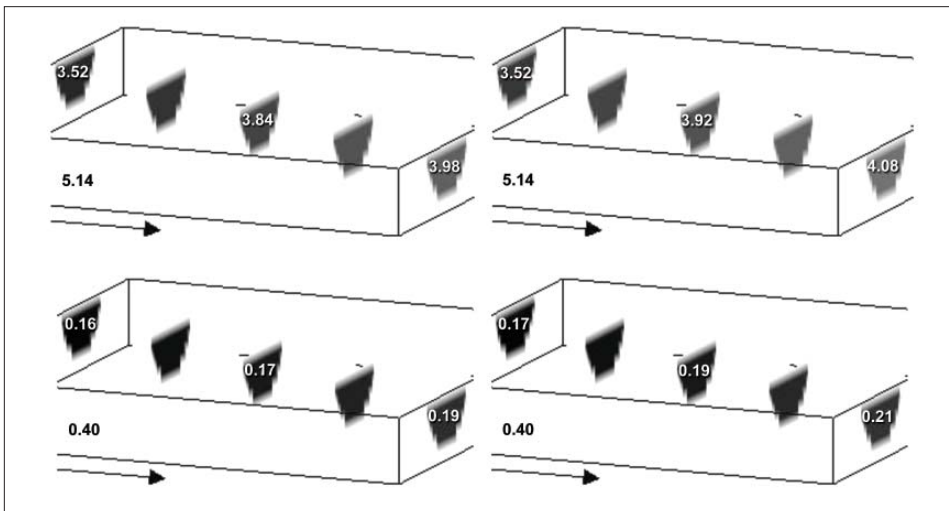


Figure 6. Acoustic impedance in kmls/gcc (top) and Poisson's ratio (bottom) for the large sand-grain scenario (left) and the small sand-grain scenario (right).

and clay content in the surrounding shale are fixed at 25 and 75%, respectively.

To assign absolute permeability to this Earth model, let us examine two scenarios: (a) $d_{\text{Sand}} = 0.40$ mm and (b) $d_{\text{Sand}} = 0.10$ mm. For both scenarios d_{Shale} is constant 0.01 mm. The mean grain size in the channel is computed from Equation 3.

Next, k_{Absolute} is computed from Equation 2 for $\phi_p = 0.025$ and $\tau = 2.5$ (Figure 5). The permeability in the shale is very small and fixed at 0.001 mD.

We observe a drastic decrease in absolute permeability along the direction of depositional flow for both scenarios, mostly due to the increase in clay content. This effect is not unexpected in light of experimental data shown in Figure 1. Also, the absolute permeability for the small grain case is from a quarter to a half of that for the large grain case.

Next, by using these results and Equation 4, we calculate the irreducible water saturation in the channel. We also assume that the water in the channel is at S_{wi} and, hence, oil saturation S_o is $1 - S_{wi}$.

The acoustic impedance and Poisson's ratio for these two cases were calculated from the soft-sand model (see the ranges of these elastic attributes versus porosity in Figure 3) and are displayed in Figure 6. Both seismic attributes are essentially the same between the two scenarios. Yet the absolute permeability is not.

Its effect on oil recovery can be captured by a single value that is the harmonic average of the relative permeability to oil k_{ro} in the direction of the channel. By assuming that k_{ro} is 0.4 of k_{Absolute} at S_{wi} (as shown in Figure 2), we calculate this value as 330 mD for the large-grain scenario and 130 mD for the small-grain scenario—a factor of 2.5 difference that will certainly affect the reservoir modeling and production forecast.

Quantifying permeability and other rock properties

A commonly used approach to populate the reservoir model with permeability is to adopt a porosity-permeability transform specific for a lithology under examination. Unlike porosity and elastic properties, permeability and, especially, relative permeability cannot be directly measured by well logging. Establishing plausible porosity-permeability trends requires special core analysis conducted in the lab and on a large

number of samples. Not only are such experiments lengthy and expensive but also there is often a lack of rock material to conduct these experiments: core can hardly be extracted from deviated wells and slim holes. The only material from such wells might be (often seriously damaged) sidewall plugs and drill cuttings.

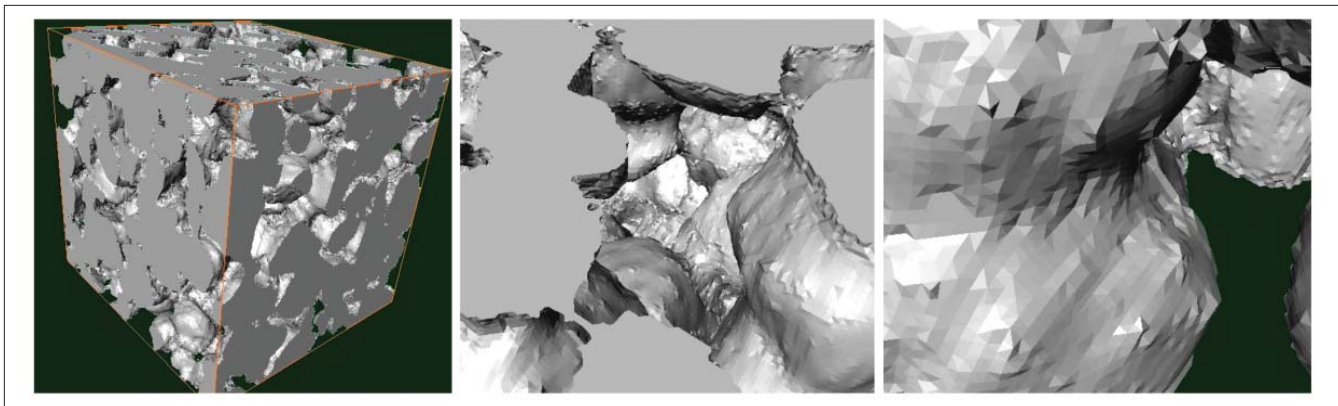


Figure 7. Micritic carbonate. The same sample displayed at increasing magnification. The images are (left to right) about 20, 8, and 2 microns across.

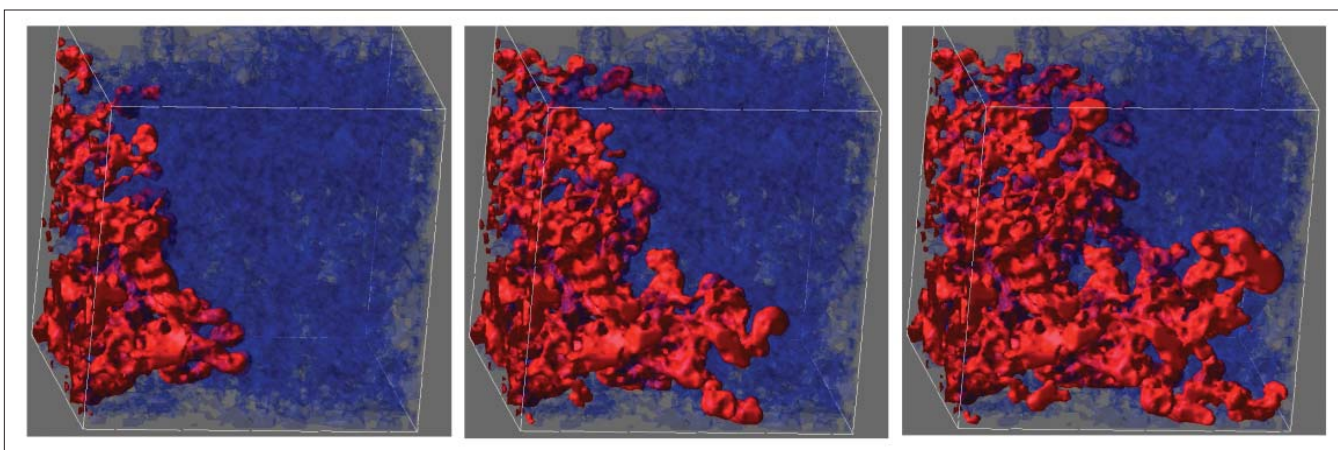


Figure 8. Two-phase flow simulation of oil imbibition in sandstone. Red = oil. Blue = water.

In such situations, computational (or digital) rock physics is the only experimental tool available. The simple principle of computational rock physics is “image and compute” which means: image a rock fragment at the pore and grain scale and then simulate physical processes, such as multiphase fluid flow, electrical conduction, and elastic deformation to arrive at permeability, conductivity, and elastic properties, respectively. Implementing this simple principle is not simple. It requires state-of-the-art imaging, image-processing, and physical-process-simulation algorithms, matched by powerful hardware.

Specifically, a computational experiment has three distinctive stages:

3D CT-scan image construction. At this stage, a sample is placed inside a CT-scan machine where it is illuminated with focused X-rays of desired frequency. This frequency determines the resolution of the image—the size of a single voxel can vary from a few nanometers to a micron and to a centimeter. The sample is mechanically rotated inside the machine to view it at all angles. The software supplied with the machine tomographically reconstructs the 3D volume. These images come in shades of gray. The gray level is directly affected by the average atomic number of the material, which is, simply speaking, its average density. For example, if the

rock fragment under examination contains dolomite, calcite, quartz, porous clay, and air in the large pores, the brightness of the voxels representing these entities will reduce from almost white for dolomite to almost black for the pores. The porous clay will appear as a darker gray because (depending on its intrinsic porosity) its bulk density is smaller than that of the pure clay mineral. In other words, although we may not necessarily resolve the individual clay particles, we will identify the clay and can estimate its porosity by assuming the density of the clay mineral which is related to the clay type. The same holds for porous micrite in carbonates. If the pores contain fluids with a significant density contrast (e.g., water and air), we can identify these fluid phases in the CT image.

A nano-CT machine can resolve small micritic grains (Figure 7). It can also resolve relatively large shale particles but not the smallest clay platelets. To image the latter, we use the FIB-SEM (focused ion beam combined with scanning electronic microscope) technique. The ion beam removes the rock material above the cutting plane and exposes a flat unaltered area, which is then imaged by SEM. Such 2D images can be obtained sequentially at extremely close planes. Then these 3D images are combined to produce a tomographic 3D image at a very high (5–10 nm) resolution.

Image segmentation. At this stage, the entire gray-scale

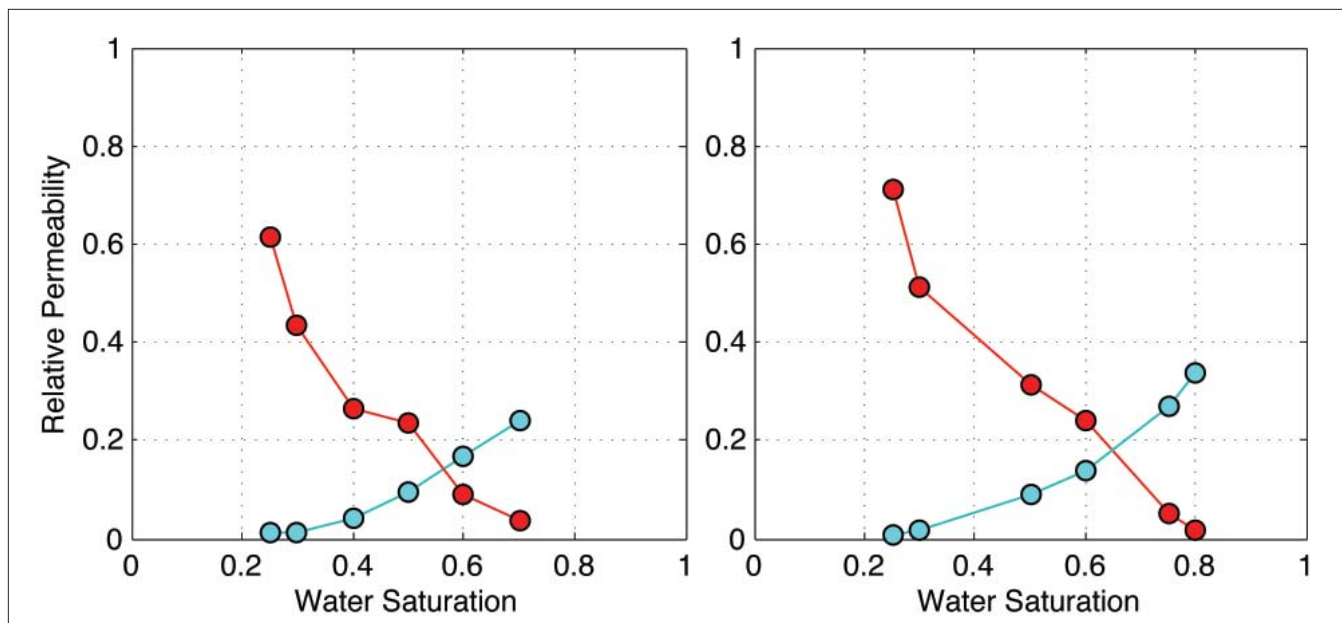


Figure 9. Relative permeability curves to water (blue) and gas (red) in the same sandstone sample but with varying interfacial tension (from left to right).

range of the image is reduced to a few integers, such as 0s for pores, 1s for quartz, and 2s for calcite. This procedure is based on fairly sophisticated image-processing algorithms (rather than simple color thresholding) and is essential for any process simulation as it strictly defines the pore space where the fluid flows and the mineral phases through which the elastic stress is transmitted. Figure 7 displays a segmented image, 0s (black) for the pores and 1s (gray) for calcite. Here the smallest features of the pore space become apparent as magnification increases.

Process simulation. After a digital image is acquired and segmented, fluid flow is simulated in the digital pore space (Figure 8) and relative permeability curves are computed (Figure 9). A salient feature of such calculations is that the pore space and mineral matrix of the segmented image are *not* replaced by an idealized geometry (as in, e.g., network modeling). Rather, the image is used directly, with all its visible intrinsic complexity intact. To achieve this goal for single- as well as two-phase fluid flow, we employ the lattice-Boltzmann computational method (LBM). LBM is based on Newtonian dynamics of particles traveling and colliding on a 3D spatial grid. With the collision rules appropriately specified, the particle speed and pressure fields precisely mimic those governed by the Navier-Stokes equations for viscous flow. The importance of LBM for fluid-flow simulation is that the no-slip boundary conditions can be implemented at the fluid-solid boundaries of any geometry (as imaged), which is essential in real pore space.

For a multiphase flow, the wettability angles, interfacial tension, and viscosities have to be specified prior to computation. This requirement can be viewed as restrictive since these inputs are not necessarily easily available. It can also be viewed as an advantage since it allows the digital experimentalist to explore variations in these inputs and, by so doing, deliver a

range in relative permeability relevant to plausible reservoir conditions as opposed to just a single answer.

The elastic properties are simulated using a finite-element method (FEM) with the elements placed in the mineral matrix and their elastic moduli assigned according to the mineral types as determined during segmentation. This is not a purely mathematical procedure as it requires a decision by a geologist and petrophysicist to select minerals appropriate to the rock under examination. Sometimes selected SEM images are taken to better understand and identify the rock.

The electrical conductivity is also computed using FEM with the elements placed in the pore space and conductive minerals. Similar to other simulations, the conductivities of the individual phases have to be specified prior to calculations.

Because these computational experiments are conducted on the same digital object and in precisely imaged pore space, it is possible to interrelate the named attributes of rock. Another unique and valuable feature of such digital experiments is their repeatability. A digital sample can be kept for as long as required and can be revisited at any time to conduct additional simulations during the entire lifespan of the field. This is difficult (if not impossible) to manage in the physical lab or in the well.

Moreover, because a stable distribution of two or more fluid phases inside a physical sample and for desired saturation is not easy to achieve, the saturation conditions in the physical lab are difficult to control. Even if the desired state of saturation is achieved in a physical sample, it is hardly reproducible. This is why multiphase flow simulations in the physical lab and the resulting relative permeability curves are sometimes difficult to interpret in terms of their relevance to in-situ processes. In contrast, the saturation conditions are straightforward to simulate in the digital lab—they directly

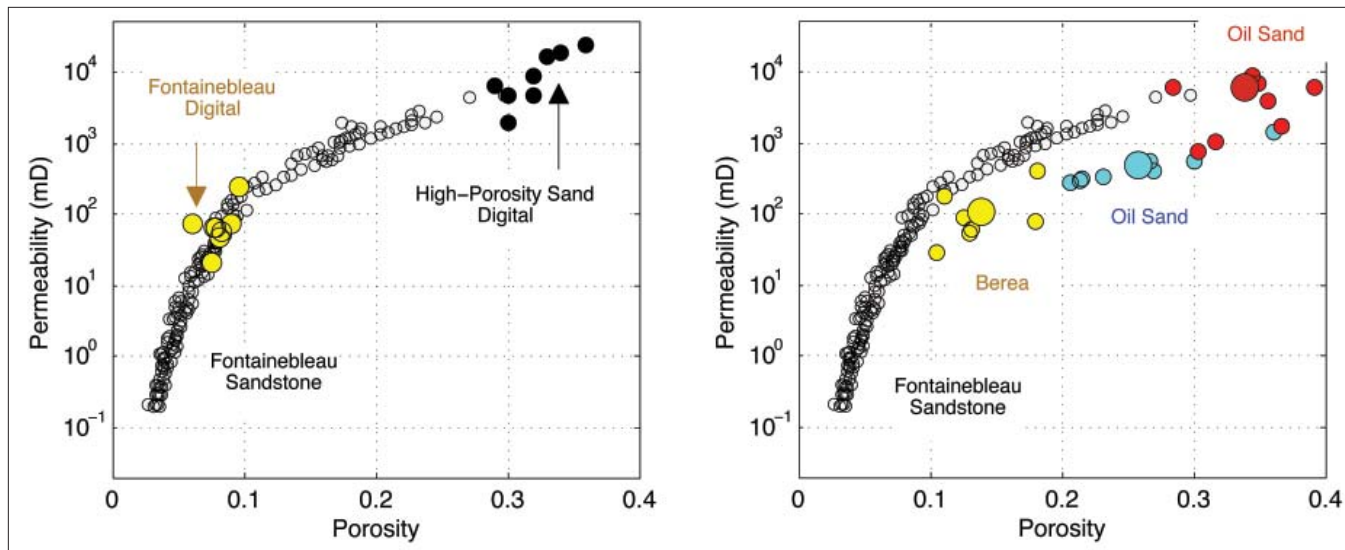


Figure 10. (left) Absolute permeability versus porosity for Fontainebleau sandstone measured in the lab (light-gray with black rims) and obtained by subsampling a single small digital sample (yellow). Black symbols are digital measurements on high-porosity sand. (right) Digital permeability-porosity trends from subsamples of Berea sandstone (yellow), oil sand A (cyan), and oil sand B (red). The larger symbols are for the original (relatively large) digital samples while the smaller symbols are for their subsamples.

evolve during the simulation for specified inputs (wettability, interfacial tension, and viscosity) once the flow with required fluxes of each phase is stabilized in time. Moreover, these conditions are easily reproducible on the same digital object for different fluid phases with varying viscosity and wettability. This capability opens up a universe of data produced for various fluid types and contents. It also helps embrace a wide range of plausible conditions in the reservoir during the initial and enhanced recovery.

The question is how relevant these digital data computed on mm-sized rock fragments are to fluid flow in a reservoir.

Scale: Do digital rocks represent real samples?

This question of upscaling is no less serious for physical-lab data than it is for the digital lab: The spatial scale in both types of experiments is orders of magnitude smaller than in the reservoir. The advantage of digital data is their massiveness. Not only can we rapidly measure many digital samples, but also by subsampling a single digital sample and thus covering ranges of porosity and textures, we can establish trends that are valid at a much larger scale and, hence, we speculate, are functional at the reservoir scale.

Consider, for example, Figure 10 where digital results for high-porosity sand and for subsampled Fontainebleau sandstone are compared to physical Fontainebleau data. Yellow symbols come from digital experiments conducted on a small digital Fontainebleau image that was numerically cut into eight subsamples. Remarkably, these digital data fall precisely on the physical experimental trend. Added to these data are also digital results from several very small samples of high-porosity sand. This digital trend continues the physical Fontainebleau trend.

More examples of consistent and physically justifiable trends from digital experiments are given in Dvorkin and Nur

(2009). We have observed similar cross-scale consistency not only for absolute permeability but also for the elastic properties of sandstone and carbonate. Subsamples of a few digital samples have allowed us to form a meaningful trend consistent with physical data and theoretical models.

It is not clear yet how to generalize digital lab relative permeability curves and how to upscale them to the reservoir level. However, this generalization will come as a result of massive digital multiphase flow simulations on samples from various formations and under realistic reservoir conditions.

Conditions: Are digital experiments usable in situ?

Rock fragment imaging occurs at room conditions. The main difference with the in-situ conditions is essentially zero differential stress. Does this disparity affect the simulation results? To address this question, we need to review existing laboratory data.

In essentially all rock types, the total porosity varies little with stress. Hence, the digital porosity of segmented rock images is approximately the same as in situ.

In medium-to-high porosity rocks, the absolute permeability and formation factor do not change much (by less than 30%) as in-situ pressure is applied to the sample. Hence, the digital permeability computed on such samples is relevant to the in-situ values.

However, in tight-gas sandstones, both the permeability and formation factor may reduce by a factor of 5–10 as large confining stress is applied. This is most likely due to the closure of microcracks generated when a sample is being brought to the surface. To mitigate this effect, we operate on a segmented image. Specifically, we mathematically close the thin cracks and leave the relative large pores intact. Then the image thus altered is used in fluid-flow or electrical-flow simulations. This operation allows us to estimate the relevant

values (if not exactly compute the in-situ permeability and formation factor). Other factors affecting permeability, such as wettability, interfacial tension, viscosity, and saturation, are directly dialed into computational experiments as input parameters appropriate to reservoir conditions.

The *elastic properties* are highly sensitive to stress. The reason is the microcracks nonexistent in situ open up at room conditions. These microscopic defects hardly affect porosity and (in most rocks) permeability but act to strongly soften a sample at small differential stress. The remedy is very similar to that used for permeability estimates in tight-gas sandstones: We mathematically close these elastic defects or, sometimes, simply try not to see them by using a relatively coarse image resolution. Our digital experiments usually provide accurate elastic-property values measured at in-situ stress.

Conclusion

The outcomes of digital experiments are affected by the inputs—mineralogy and fluid chemistry, and how they interact to affect wettability and surface tension—not just information about the pore structure. To reliably forecast reservoir processes we need this solid-phase and fluid-phase information. This situation is not very different from traditional reservoir simulation where such information is essential as well and comes either from laboratory analyses of reservoir fluids or accumulated petroleum engineering knowledge.

The power of digital experiments is that they can be conducted repeatedly on the same object for a range of these inputs. Hence, we can embrace a plausible range of reservoir responses. Moreover, by displacing fluid phases in the same digital sample in specified succession, we can quantify potentially important effects, such as hysteresis in relative permeability.

The reliability and relevance of digital data are usually evaluated by comparing these results to laboratory data obtained on a similar rock type and also to theoretical models. For some rock types, digital data appear to be more reliable than for others: The computed permeability closely matches laboratory data in medium- to high-quality reservoir rock (permeability higher than 1 mD). In low-permeability samples where the pore space is occluded by clays or relatively large pores appear disconnected but in fact are connected by thin conduits, careful imaging of these subtle features is required. Our experience indicates that once we image such features, the digital data become reliable. In other words, we can only compute what we image, and this is an important (and manageable) challenge in digital rock physics.

Digital experimentation is a powerful means of obtaining massive site-specific trends between rock properties. Such trends obtained at a sub-mm scale are still consistent with rock physics models and physical measurements. This cross-scale consistency leads us to speculate that the same trends may be applicable at the reservoir scale. This is especially valuable for permeability since digital data can be produced from almost any available rock material, including cuttings.

By no means is digital experimentation intended to eliminate laboratory or well measurements. Its aim is to enrich such data as well as extend physical databases far beyond the properties and conditions used in the laboratory, as well as to reduce to the minimum the number of complicated physical measurements as required for digital data calibration and verification.

Suggested reading. *Quantitative Seismic Interpretation* by Avseth et al. (Cambridge, 2005). “Scale of experiment and rock physics trends” by Dvorkin and Nur (*TLE*, 2009). Effects of Porosity and Clay Content on Acoustic Properties of Sandstones and Unconsolidated Sediments by Han (PhD thesis, Stanford University, 1986). “The effect of a percolation threshold in the Kozeny-Carman relation” by Mavko and Nur (*GEOPHYSICS*, 1997). *Rock Physics Handbook*, 2nd edition, by Mavko et al. (Cambridge, 2009). Acoustic Velocity and Attenuation of Rocks: Isotropy, Intrinsic Anisotropy, and Stress-Induced Anisotropy by Yin (PhD thesis, Stanford University, 1992). **TLE**

Acknowledgments: We thank Reinaldo Michelena and Emmanuel Gringarten for their constructive comments and suggestions.

Corresponding author: dvorkin@stanford.edu